In-Vitro Imaging Of Thermal Lesions Using Three Dimensional Vibration Sonoelastography

L.S. Taylor*, M. Zhang† , J.G. Strang**, D.J. Rubens* and K.J. Parker*

*University of Rochester, ECE Department, Rochester NY
†University of Rochester, BME Department, Rochester NY
**University of Rochester, Radiology Department, Rochester NY

Abstract. HIFU and radio frequency (RF) ablation are methods for treatment of cancerous lesions which create a coagulation necrosis killing the undesirable cells. A technique for real time monitoring of HIFU lesions would be a useful adjunct to this therapy. Sonoelastography is being investigated as a real time monitoring method. Fresh bovine liver was degassed and RF ablation was used to induce a coagulation necrosis in the liver. Three dimensional sonoelastography images were acquired. After imaging, lesions were dissected to document their size, shape and volume.

Upon dissection the induced lesions were all found to be palpably hard, ellipsoidal in shape and of differing texture and color than the untreated tissue. The mean volume of the five lesions determined by fluid displacement was 4.7 cc. In the sonoelastography images each lesion appeared as a dark region surrounded by a field of bright green. The precise edge of each sonoelastography lesion was somewhat ambiguous, +/- a few mm. The mean sonoelastography volume for the five lesions was found to be 87% of the volume determined by fluid displacement when only the lowest vibration amplitude region was taken to represent the lesion. Real time monitoring of thermal lesions can be accomplished *in-vitro* by making the sonoelastography lesion equal to the desired treatment zone.

INTRODUCTION

High intensity focused ultrasound (HIFU) and radio frequency (RF) ablation are both used for non-invasive tissue ablation treatments. Often the objective is to create a coagulation necrosis lesion at the site of an existing and known malignant lesion. Real time monitoring of these lesions is a major challenge for the application of these methods in a clinical setting. Ultrasound B-mode imaging is often used for probe placement but the hyperechoic zones seen during treatment correspond only weakly with the extant of the tissue necrosis [1]. Computed tomography (CT) and magnetic resonance (MR) imaging can be used but their size, cost and relative immobility limit their usefulness [1].

Several approaches to this problem are under active investigation and capitalize either on the fact that tissue temperatures rise during the treatment process or that coagulation necrosis lesions have an elevated Young's modulus relative to the untreated tissue. Stafford et al. [2] used elastography to visualize thermally induced lesions *in-vitro*. A surgical laser was used to create thermal lesions in ovine kidney. Elastography images of the treated kidneys revealed reduced strain levels in the lesion area as confirmed later by histology. In a subsequent study at the same institution Righetti et al. [3] used high intensity focused ultrasound to induce thermal lesions in canine livers. The strain

images showing the lesion location were validated by photographs of the dissected livers. Konofagou et al. [4] have proposed using ultrasound stimulated vibroacoustography [5] to monitoring tissue ablation. Since the ultrasound stimulated acoustic emission depends on the temperature it can be used for localized temperature detection.

Sonoelastography has been previously proposed as a method of imaging the relative elastic properties of soft tissues [6]. In this technique, low frequency shear waves (0 - 1000 Hz) are propagated through tissue while Doppler vibration detection methods [7] are used to image the resulting vibration field. Under the correct boundary conditions [8, 9], regions in the image with an elevated elastic (shear or Young's) modulus, will appear as regions of decreased vibration indicating the location of the stiffer tissue. We have demonstrated this technique in phantoms containing hard lesions [10, 11].

In this paper we propose sonoelastography imaging as a method for the real-time imaging of coagulation necrosis lesions. RF ablation lesions are used as a model for coagulation necrosis lesions. We show that real-time sonoelastography images can accurately detect the location and size of these lesions. Details on how to implement this technique are provided.

MATERIALS AND METHODS

In this section details on the various materials used to validate real-time imaging of thermal lesions will be presented, including the liver specimens, embedding materials, RF ablation equipment, vibration sources and ultrasonic scanner. After this the experimental set-up will be described along with methods used for specimen embedding, lesion creation, application of the vibration, three-dimensional 3D image acquisition, lesion dissection and lesion volume calculation from the sonoelastography images.

Materials

Whole fresh bovine liver was purchased from a local butcher (Wegmans Food Market, Pittsford, NY). The liver was immersed in a degassed 0.9% NaCl solution and stored at approximately 4^o C for 24-36 hours. Tissue samples ($\approx$ 10 x 10 x 6 cm) were cut and soaked in the degassed saline solution before sonoelastography imaging. This process avoided large bubbles in the tissue which would have an ill effect on image display.

DIFCO^{TM} Technical Agar (Becton Dickinson, Sparks, MD) was used to create 2.25% agar molds embedding bovine liver samples. The mechanical characteristics of 2.25% agar molds were similar to the liver tissue at the vibration frequencies used, which was verified by prior research.

Thermal lesions were induced in liver tissue samples using (RF) ablation. Figure 1 shows a *LeVeen*^{TM} needle (RadioTherapeutics Corporation, Mountain View, California, USA) of 15 cm in length along with a centimeter scale. The umbrella-shaped tines are extended and a RF current which is generated by a RF ablation machine (RadioTherapeutics Corporation, Mountain View, California, USA) passes through the needle tip to the target tissue. The current is returned by means of four attached grounding pads

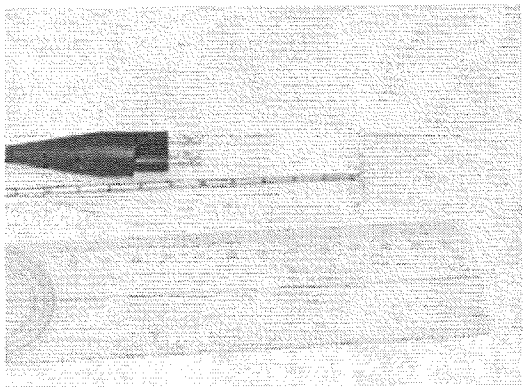

FIGURE 1. Needle used for the RF ablation process.

connected back to the machine through electric cables. This equipment is used clinically in liver cancer therapy at our institution.

A GE Logiq 700 (General Electric Medical Systems, Milwaukee, WI) ultrasound scanner was used to perform sonoelastography imaging. The scanner was specially modified so that the Doppler spectral variance of the vibrating tissue is mapped to the screen in color mode when the appropriate color map is selected. Huang et al. [7] have shown that the standard deviation of the power spectrum depends directly on the vibration amplitude of the tissue. In order to acquire three-dimensional images, a 7-MHz linear array transducer (739L GE Medical) was mounted and aligned in the holder of a motorized linear track.

In preparation for imaging, the embedded specimens were placed on two thin parallel bars which were separated by 5 cm on center. The purpose of using the two parallel bars as a vibration source was twofold, to produce a uniform vibration and to focus and concentrate the shear wave production into a region of interest [12]. The twin bar assembly was in turn mounted on a 100 lb. (force) piston shaker (VTS Aurora, OH) which provided the low frequency vibration field required for the vibration imaging. The shaker was driven by an audio amplifier whose voltage output waveform could be precisely controlled by a frequency generator. A harmonic waveform generator (3511A, Pragmatic Instruments, San Diego, CA) was used to provide multi-tone vibrations.

Methods

Figure 2 shows the experimental setup used for imaging RF ablation lesions. Two parallel bars were applied at the center of the bottom surface of the agar embedded specimen and low frequency multi-tone vibration was used to drive the shaker. The transducer was used to locate the lesions of interest in the phantom. The color Doppler mode of the modified GE Logiq 700 ultrasound system was used for image display.

The proper mass of agar powder was weighed and added to the near boiling degassed H_2O (2.5 liters), which was stirred when adding the agar until most of agar was dis-

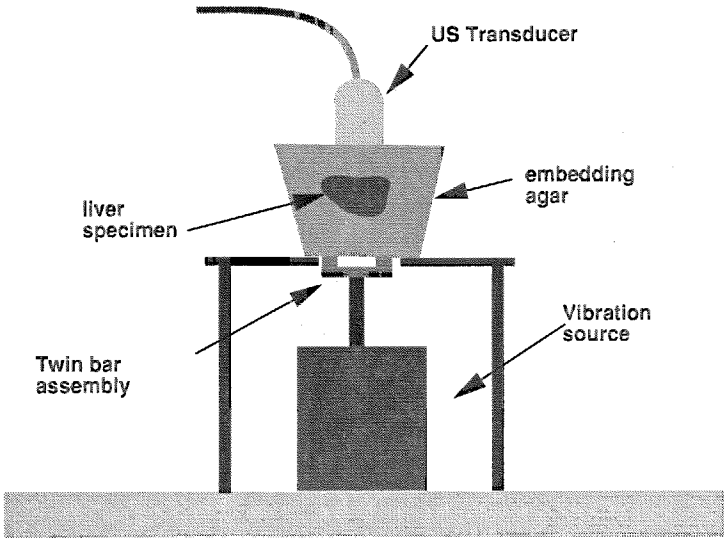

FIGURE 2. Experimental Set-up.

solved. Then this solution was boiled again in a microwave. Deviation from this procedure sometimes resulted in an agar mixture which did not gel properly. The solution was allowed to cool to $\approx 70^{o}C$. Then 1.7 liters of the solution was poured into a 2.5-liter $Ziploc^{TM}$ bowl-shaped container. Another smaller cylindrical container ($\approx$ 10 cm in diameter) was inserted into the solution to create a cavity 8 cm in depth in the center.

After 2 hours in the refrigerator, the agar shell was created and the liver sample was put into the cavity. The remaining 0.8 liter agar gel was remelted and boiled. It was allowed to cool but not harden, and poured into the cavity to embed the liver sample completely. In this step, bubbles should be removed from the agar solution carefully. The whole mold was allowed to harden for an hour before the insertion of the $LeVeen^{TM}$ needle.

From the screen of the ultrasound scanner, we could control and adjust the depth and direction of the needle. The optimal insertion direction would be 45^{o} between the needle and the mold surface. The insertion depth was about 5-6 cm beneath the mold surface. This RF ablation process heated the tissue, successfully making a lesion centered at the needle tip. The process required about 150 seconds for completion.

In order to image the lesions using sonoelastography, the scanner was placed into color Doppler mode and the multi-tone vibration source was activated to drive the double bar assembly. Multi-tone signals were used to reduced the modal artifacts which occur during *in-vitro* imaging because of specular reflection of the shear waves off of the specimen holder boundaries [13]. On this scanner the estimated vibration field is mapped to a gray scale where high vibration is bright and lower vibrations are dark. By observing the location of the dark pixels, it was possible to located the stiffer tissue, which vibrates at a lower amplitude. The location of the lesions was also possible using the B-scan image which showed the needle track and gas bubbles from the ablation process. In

order to acquire 3D sonoelastography images, the linear track holding the transducer was activated so that the velocity of the motor was synchronized to the frame rate of the scanner so that images were acquired at a fixed spatial interval of 1 mm. The sequence of images was saved as a cine-loop of co-registered B-mode and sonoelastography images.

After image capture the files were transferred from the scanner's hard drive to an image processing laboratory via a network connection. Both the two-dimensional (2D) and 3D sonoelastography images display areas of decreased vibration as dark gray or black. The sonoelastography images of the lesions were manually segmented using the ImageJ software package from NIH to calculate lesion area in each slice. The vibration deficit in each image was outlined and ImageJ was used to calculate the area . After outlining, the lesion was filled in and the sonoelastography image was converted to a binary image where the lesion was white and the background was black. The sequence of binary 2D renderings of the lesion was imported into IRIS Explorer, a 3D visualization package to create a 3D rendering of the lesion. Since images were acquired at 1 mm intervals the volume was estimated using a cylindrical approximation multiplying the thickness of the slice by the area of the lesion in each slice.

After imaging, the lesion sizes were verified by removing them from the embedding agar and cutting away the soft untreated tissue from the hard thermal lesions. Their volumes were then measured by two methods. The typical shape of a thermal lesion was ellipsoidal and the texture and color of it are different from the surrounding normal tissue, which facilitated accurate determination of the thermal necrosis. Caliper measurements were applied to measure the three maximum axes of a dissected lesion, using an ellipsoidal geometrical model. The volume, V, of each lesion was calculated by the formula:

$$V = \frac{4}{3}\pi xyz, \tag{1}$$

where x, y and z are the half lengths of the three axes.

The volume of each lesion was also determined by fluid displacement. In this method, a dissected lesion was placed into a water filled vessel whose displacement indicated the volume of the lesion.

The vibration deficit in each (sonoelastography) image was an ellipsoidal-shaped dark area. The longest two axes were measured from the slices in which the dark area was largest compared to the others in the sequence. The third axis was determined by counting how many slices contained a deficit in vibration. This established the tumor size in the out of plane direction. The volume could then be estimated from the total thickness of all slices containing lesions and the lengths of the two principal in plane axes described above using equation 1.

RESULTS

Figure 3 shows a typical RF ablation lesion after it has been dissected. Measurements of five lesions are given in Table 1. The volume of each dissected lesion was determined by caliper measurements and fluid displacement. The lesion dimensions and image volumes of the same lesion were observed and calculated from the sonoelastography images.

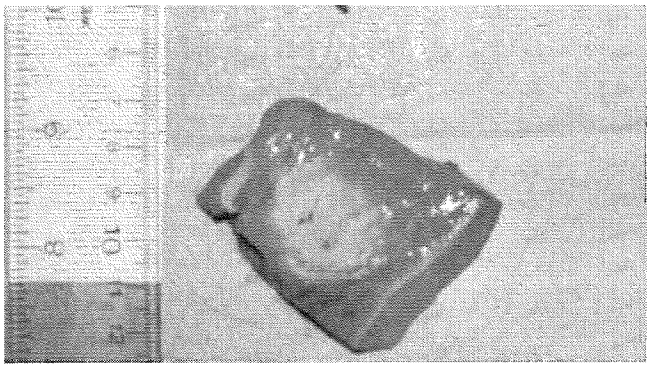

FIGURE 3. Dissected RF lesion.

In the sonoelastography images each lesion appeared as a dark region surrounded by a bright field. In our experiments, only the darkest pixels were taken to represent the lesion. However, the exact edge of each sonoelastography lesion was somewhat unclear. If the largest possible regions were used in measurements, the dimensions and image volumes of the five lesions would be much larger than those of the dissected lesions. We found that the volume of each dissected lesion was between the sonoelastography volume with only the darkest pixels taken into account and that with the largest possible region. The sonoelastography volumes for the five lesions were smaller than the volumes determined by fluid displacement. The mean percentage was 87% . In Table 1 the column marked *Caliper Volume* refers to the volume estimated from the caliper measurements using Equation 1, *Caliper Msr* , refers to caliper measurements on the dissected lesion, *Fluid Vol* gives the true volume determined by fluid displacement, *Sono Axes* are the lesion dimensions from the 3D sonoelastography images, *Sono Volume Axes* refers to the volume calculated using the axes measured in the sonoelastography images and *Sono Volume* refers to the lesion volume estimated by segmenting the 3D sonoelastography image set.

Figure 4 shows three lesions imaged using sonoelastography. Shown from left to right are lesions 1, 2 and 3. The arrows mark the location of the thermal lesion in the image.

TABLE 1. Measurements on Five Lesions.

	Caliper Volume cm	Caliper Msr cc	Fluid Vol cc	Sono Axes cm	Sono Volume Axes cc	Sono Volume cc
1	4.8	3.0 x 1.9 x 1.6	4.8	2.6 x 2.1 x 1.6	4.5	4.4
2	4.2	2.5 x 2.0 x 1.6	4.2	2.3 x 2.2 x 1.5	4.0	3.8
3	4.9	2.8 x 2.1 x 1.6	4.6	2.6 x 2.2 x 1.3	3.9	3.6
4	4.6	2.6 x 2.1 x 1.6	4.4	2.5 x 2.1 x 1.5	4.1	3.9
5	5.4	3.0 x 2.3 x 1.5	5.4	2.9 x 2.4 x 1.5	5.5	4.6

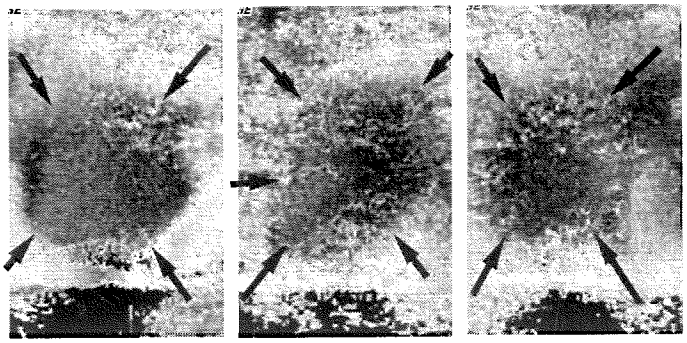

FIGURE 4. Three RF Lesions imaged using sonoelastography.

Each of these images were taken in the plane of the ablating needle. It was from these images that the first and third numbers in column *Sono Axes* of Table 1 were measured. The second number in that column is the out of plane thickness of the lesion.

Figure 5 shows co-registered B-mode and sonoelastography images of lesion 4, taken in the plane of the ablating needle. The needle is visible in the B-mode image (A) entering the image in the middle left hand side and ending at the lesion. In the sonoelastography image the lesion is clearly visible as a dark region. The lesion boundary determined by the sonoelastography image has been superimposed on the B-mode image.

Figure 6 shows a 3D sonoelastography rendering of lesion 3. Each image in the sequence of 2D sonoelastography images was segmented into tumor and background, then imported into IRIS Explorer and rendered as a 3D object. The field of view shown is contained with a bounding box of 2.8 x 2.1 x 1.6 cm.

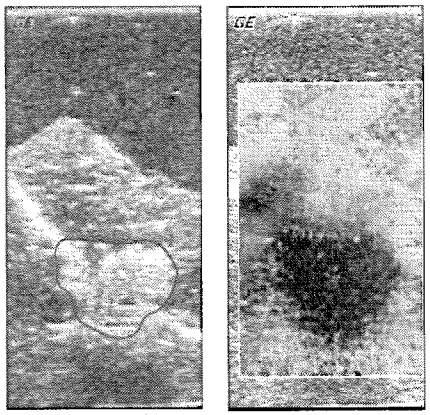

FIGURE 5. Lesion 4 B-mode image (A) and sonoelastography image (B).

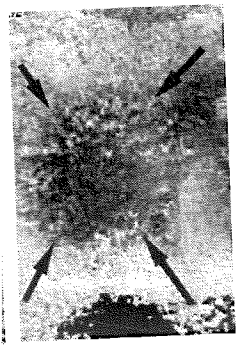

3

ing sonoelastography.

ablating needle. It was from these
no Axes of Table 1 were measured.
e thickness of the lesion.
stography images of lesion 4, taken
ble in the B-mode image (A) enter-
g at the lesion. In the sonoelastogra-
on. The lesion boundary determined
sed on the B-mode image.
ng of lesion 3. Each image in the
nented into tumor and background,
3D object. The field of view shown
cm.

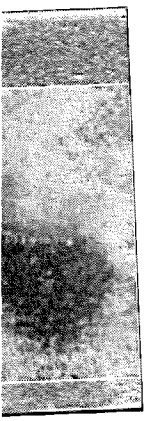

B

id sonoelastography image (B).

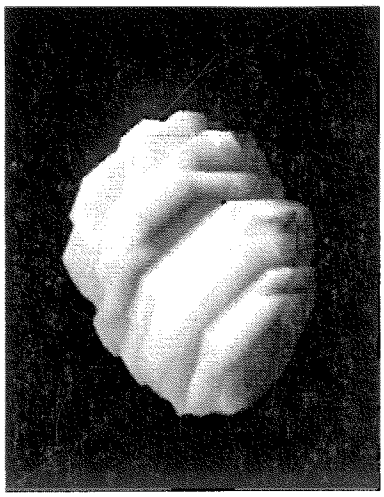

FIGURE 6. 3D Rendering of Lesion 3.

DISCUSSION

We have used RF ablation of healthy bovine calf liver as a model for coagulation necrosis lesions in general, and have shown that such lesions appear very clearly in sonoelastography lesions. In the clinic the goal of RF ablation is to generate an coagulation lesion whose diameter is equal to or greater than that of the tumor. Since sonoelastography images the relative elastic properties of tissue, when imaging a tumor which is itself stiff the contrast between the thermal lesion and the tumor may not be as high as suggested in Figure 4.

Our observation that the lesion boundaries in the sonoelastography images were somewhat ambiguous suggests two alternative explanations. First, it might be that the boundary between the normal tissue and thermal lesion is quite sharp and the ambiguity is a result of the vibration field at the boundary. Second, it might be that the variation in the tissue elastic modulus across the boundary itself varies slowly in the spatial dimension and the sonoelastography image is reflecting that variation in modulus. It seems reasonable to assume that the ablation in the tissue depends on the local density of RF current during the ablation process. Since current originates at the needle's tines and spreads out more or less spherically, it is safe to assume that the current flux density falls off with the radius, r, from the needle point as $1/r^2$. If the increase in local elastic modulus is proportional to the square of the current (i.e. energy flux) and the overall temperature-time history produced at a point, leading to heat denaturing of proteins, it could be that the boundaries themselves are more ambiguous than suggested by the photograph of a dissected lesion shown in Figure 3. Based on our prior work on imaging hard lesions in phantoms cited in the introduction, we find support for the second explanation, as phantom lesions show sharp boundaries whenever vibration artifacts were properly controlled.

SUMMARY AND CONCLUSIONS

Sonoelastography imaging of thermal induced lesions in liver tissue has been verified. Two-dimensional sonoelastography images through the plane of the ablating needle showed deficits of vibration centered at the end of the needle track. From this it is concluded that sonoelastography effectively detects thermal lesions in soft tissue. Dissection of the thermal lesions verified that they were palpably harder than the surrounding tissue. The true size of the lesion can be accurately estimated from the 3D images. Sonoelastography may be useful as a means of real-time monitoring of thermal lesion formation.

ACKNOWLEDGMENTS

This work was supported in part by the University of Rochester Departments of Radiology and Electrical Engineering, the General Electric Company (GE) and NIH grant 2 RO1 AG16317-01A1. The authors thank GE Medical Systems Division for the loan of the scanner used in the imaging experiments. The authors thank Clark Zhe Wu for his suggestions on using the needle axis as a basis for the lesion measurement coordinate system.

REFERENCES

1. Gazelle, G., Goldberg, S., Solbiati, L., and Livraghi, T., *Radiology*, **217**, 633–646 (2000).
2. Stafford, R., Kallel, F., Hazle, D., J Cromeens, Price, R., and Ophir, J., *Ultrasound in Med. & Biol.*, **24**, 1449–1458 (1998).
3. Righetti, R., Kallel, F., Stafford, R., Price, R., Krouskop, T., Hazle, J., and Ophir, J., *Ultrasound in Med. & Biol.*, **25**, 1099–1113 (1999).
4. Konofagou, E., Thierman, J., Karjalainen, T., and Hynynen, K., *Ultrasound in Medicine and Biology*, **28**, 331–338 (2002).
5. Fatemi, M., and JF, G., *Science*, **280**, 82–85 (1998).
6. Parker, K., Huang, S., Musulin, R., and Lerner, R., *Ultrasound in Med. & Biol.*, **16**, 241–246 (1989).
7. Huang, S., Lerner, R., and Parker, K., *J Acoust Soc Am*, **88**, 310–317 (1990).
8. Gao, L., Alam, S., Lerner, R., and Parker, K., *J Acoust Soc Am*, **97**, 3875–3886 (1995).
9. Parker, K., Fu, D., Gracewski, S., Yeung, F., and Levinson, S., *Ultrasound in Med. & Biol.*, **24**, 1437–1447 (1998).
10. Taylor, L., Porter, B., Rubens, D., and Parker, K., "3D sonoelastography for prostate tumor imaging," in *Proceedings of the International ICSC Congress on Computational Intelligence: Methods and Applications*, ICSC Academic Press, 1999, pp. 468–472.
11. Taylor, L., Porter, B., Rubens, D., and Parker, K., *Physics in Medicine and Biology*, **45**, 1477–1494 (2000).
12. Wu, Z., Taylor, L., Rubens, D., and Parker, K., *Journal of the Acoustical Society of America*, **109**, 439–446 (2002).
13. Taylor, L., Rubens, D., and Parker, K., "Artifacts and artifact reduction in sonoelastography," in *2000 IEEE Ultrasonics Symposium Proceedings*, IEEE, 2000, pp. 1849–1852.

The Effects C
HIFUS Be

James E. Ker

*Dept. of Urology, Churc
†Dept.
‡Joint Dept. of Phy

Abstract. There are no p
ultrasound (HIFUS) focal p
safe and effective treatmen
effects on overlying ribs.
experimentally the focal pre
the HIFUS beampath. Resul
vivo to correspond with thes
Experimental and model
profile and peak intensity va
directing the beam axis thr
lying beneath the ribcage.
HIFUS doses, even though
the temperature rise on the ri
the focal plane. These experi
shielded by acoustic absorb
model should allow predictio

High-intensity focuse
centres, where tumours are
kidneys [1]. The anatomical
passes either close to the co
reflects work that is current
for major obstacles such as
the impact that more comm
size, shape or position of th
effects that the HIFUS bea
adequate treatment and to m
In some circumstances
order to provide an acoustic